

Visibility of Ink Dots as Related to Dot Size and Visual Density

Ming-Shih Lian, Qing Yu and Douglas W. Couwenhoven
Electronic Imaging Products, R&D, Eastman Kodak Company
Rochester, New York

Abstract

The light cyan and light magenta inks are used in some six-ink inkjet systems to reduce the ink dot visibility and render smooth tones in the highlight image areas. In highlights, it is believed that the drop size and visual density are the two most important design parameters affecting the ink dot visibility. To quantify this functional relationship, a psychophysical experiment was carried out to measure the threshold viewing distance as a function of the visual density for uniform light cyan patches halftoned to about 7% coverage and printed with dots having diameter of around 460, 68, and 54 microns, respectively.

By following the work of Parker and his coworkers,^{1,2} a metric (C_j), namely the standard deviation of the perceived lightness divided by the mean perceived lightness, is used to predict the dot visibility of a halftoned pattern of low-density uniform field. To compute the perceived color appearance attributes of the halftone image, the color visual difference predictor (CVDP) developed previously for the continuous-tone images is employed here. The predicted values of the threshold viewing distance for dot visibility with $C_j = 0.0021$ is found to agree reasonably well with the measurements. The results show that the parameter C_j is a proper metric for the dot visibility prediction. The model predicted results of the threshold viewing distance as a function of the dot size and its visual density should provide valuable guidance to inkjet system designers in selecting the proper settings for the drop size and ink density.

Introduction

Some inkjet systems in the market use six inks for making photographic quality prints. Typically, these inks are dark cyan, light cyan, dark magenta, light magenta, yellow, and black. The light cyan and magenta inks are mainly used to reduce ink dot visibility and render smooth tones in highlight image regions.

It is believed that the two most important design parameters that affect the ink dot visibility in highlights are drop size and density. The concentration of the light ink is usually determined via some iterative empirical exercise. The density selection and drop size setting are not two independent processes. For example, as ink drop size becomes smaller and smaller, we may be able to raise the

density of the light ink without increasing the ink dot visibility. Vice versa, as ink density of the light ink becomes lower and lower, we may be able to use a larger ink drop without increasing the ink dot visibility. It is believed that higher density light inks and larger ink drop sizes are both to the advantage of robust system design.

By following the work of Yu et al.¹ and Wang and Parker² on the texture visibility of halftone patterns, a psychophysical experiment was carried out to quantify the effects of drop size and density on dot visibility. With light cyan halftone patches of uniform field at several low densities as test samples, we measured the threshold viewing distance at which the isolated ink dots became just visible/invisible. A metric similar to what was proposed by Wang and Parker, and defined in terms of the perceived images, is introduced to predict the dot visibility. The perceived halftone images are computed by using the CVDP.³ In the following sections, the psychophysical test procedure, model computations, and method of expanding the experimental results are reported.

Psychophysical Experiment

Overview

In this experiment, uniform halftone patches were displayed, and a subject was asked to vary their viewing distances until the isolated ink dots in the patches became just visible/invisible. That specific viewing distance was recorded. This process was repeated for several patches.

Stimulus

The first set of stimuli was generated using an inkjet simulation model and a Kodak 1800-dpi continuous-tone laser thermal printer. Because ink dots are most visible at the light end of the tone scale, a typical uniform light cyan patch was selected. The uniform cyan patch was halftoned with a blue-noise dither matrix. The output halftone pattern had an ink dot coverage of ~7%.

An inkjet model was used to generate a high-resolution bitmap of the halftone pattern. For this study, all the settings were fixed except the ink concentration. Five concentrations of cyan dye at 5%, 7.5%, 10%, 15%, and 20% were selected for the printer. This resulted in five bitmaps, which were used to print five distinct patches as the stimuli.

The five patches were measured using a microdensitometer for average visual density and the ImageXpert system (ImageXpert Inc., Nashua, New Hampshire) for average size and gray value of the isolated ink dots. The measured data are listed in Table 1. We note that ink dots from different patches have different densities, but similar sizes.

Table 1. Measured Data for the Average Dots on the First Set of Stimuli.

Patch	#1	#2	#3	#4	#5
Concentration (%)	5	7.5	10	15	20
Visual Density	0.061	0.085	0.121	0.169	0.209
Diameter (μm)	463.9	446.8	458.7	459.5	474.4
Gray Value	199.6	182.7	152.6	128.5	115.8

The second set of samples having a halftone pattern with ~6% coverage of "on" pixels was printed using light cyan ink drops of 10 pl and 20 pl, respectively on a Kodak inkjet breadboard. Because of the limitation of the microdensitometer for measuring small ink drops, these two printed samples could only be measured with the ImageXpert system. Because their gray values were close to some of the patches in Table 1, their average visual densities could be estimated as 0.09 and 0.11, respectively, for the 10 pl and 20 pl drops. Their corresponding dye concentrations were 8.2 and 10.2. The results are summarized in Table 2. Figure 1 illustrates the bitmaps captured from the ImageXpert system for the #5 and 20 pl samples.

Table 2. Measured and Derived Data for the Average Dots on the Second Set of Stimuli.

Patch	10 pl sample	20 pl sample
Concentration (%)	8.2	10.2
Visual Density	0.09	0.11
Diameter (μm)	53.9	68.0
Gray Value	178.0	160.1

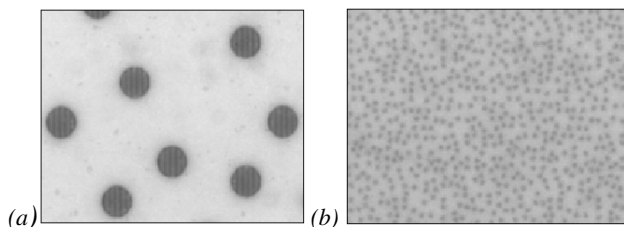


Figure 1. Bitmaps captured from the ImageXpert system for (a) patch #5 and (b) 20 pl sample.

Subjects

Seven researchers at Kodak Research Laboratories, all with normal acuity (some with corrective lenses), took part in the psychophysical experiment. Before the experiment, each individual was tested to identify his actual 20/15 vision distance. This was the longest distance at which the subject

could accurately tell at least 9 out of 10 characters in the 20/15 line on a Snellen eye chart. These data are shown in Table 3. The average distance is about 213.9 inches, which could be used as the 20/15 distance for a "normal" subject. These data were later used as normalizing factors in the section for experimental results.

Table 3. 20/15 Distance for the Seven Subjects.

subject	DC	RM	PK	PB	BZ	AZ	JY
20/15 distance (inch)	254	209	253	193	212	178	198

Procedures

All the printed halftone patches were posted in random sequence on a wall with neutral background. A continuous-tone patch of the same size and density, using the same printer, was posted next to each halftone patch. This helped the subjects discount certain printer and viewing artifacts, and concentrate on the visibility of isolated ink dots. The test site had D50 illumination with minimal visible glare.

The experiment was conducted in two phases for each observer. In the first phase, each subject stood at a distance such that no isolated ink dots were visible for all the five patches. The subject was then asked to walk toward a patch until isolated ink dots in that patch just became visible. In the second phase, each subject stood at a distance such that all isolated ink dots were visible for all five patches. The subject was asked to walk away from a patch until isolated ink dots in that patch just became invisible. Each patch was repeated three times in each phase.

Experimental Results

Each subject had six threshold distance measurements (3 in forward phase and 3 in backward phase) for each individual patch, from which both average distance and standard deviation were calculated. These data are shown in Tables 4 and 5. We note that the intra-subject variability is reasonably low for all the subjects.

Table 4. Average Threshold Distance in Inches for Each Patch by Each Subject.

subject	DC	RM	PK	PB	BZ	AZ	JY
patch #1	43.0	47.2	43.5	41.8	38.7	31.3	39.3
patch #2	82.0	74.0	90.0	66.0	68.2	51.3	61.0
patch #3	103.8	100.7	100.2	92.2	89.2	73.0	87.0
patch #4	132.5	117.5	119.3	107.7	102.5	86.8	113.2
patch #5	148.7	148.7	135.0	125.8	113.0	103.5	137.2

Table 5. Standard Deviation of Distance Measurement in Inches for Each Patch by Each Subject.

subject	DC	RM	PK	PB	BZ	AZ	JY
patch #1	2.1	2.6	6.5	5.4	2.0	0.8	2.9
patch #2	2.7	5.6	7.2	6.3	3.4	4.3	7.3
patch #3	8.4	5.7	11.0	6.1	5.2	5.0	8.8
patch #4	5.2	7.2	17.3	8.0	6.0	5.0	8.7
patch #5	5.8	5.4	12.7	18.4	5.8	8.7	7.7

The values of the normalized average threshold viewing distance as computed from Table 4 are 41.0, 70.1, 92.7, 111.7, and 131.1 inches for patch #1, #2, #3, #4, and #5, respectively. The corresponding values of standard deviation accounting only for variations among subjects are 4.8, 5.3, 7.3, 9.0, and 15.6 inches. Visual assessment of the two printed samples from the inkjet breadboard put the threshold viewing distance at 4 to 5 inches for the 10 pl ink drop and 9 to 10 inches for the 20 pl ink drop.

Model Predictions

A Metric for Dot Visibility

Based on de Vries-Rose law of the human visual threshold-versus-intensity (TVI) curve, Wang and Parker² proposed a halftone texture visibility metric as

$$C_{wp} = (\sigma_{o1} + \sigma_{o2} + \sigma_{o3}) / \sqrt{Y} , \quad (1)$$

where σ_{o1} , σ_{o2} , and σ_{o3} are the standard deviations of the signals perceived by the human visual system in the opponent color space and Y the CIE tristimulus Y value.

In the present study, we deal only with (1) monotone images that are well characterized with the signals in the perceived lightness (J) channel and (2) reflection prints for which Weber's law prevails. Accordingly, Eq. (1) is modified to yield a new metric for dot visibility as

$$C_j = \sigma_j / J_{avg} , \quad (2)$$

where σ_j and J_{avg} are respectively the standard deviation and mean of the signal in the perceived lightness channel.

A Human Visual processing Model

The color visual difference predictor³ has been developed previously to evaluate the perceived differences among continuous-tone images. It consists of a cone response model by Hunt,⁴ a filter set of contrast sensitivity functions (CSFs) by Daily,⁵ the modified Cortex Transformation by Watson⁶ and Daly⁵ for multichannel spatial decomposition, a multichannel interaction model by Singer and D'Zmura⁷⁻¹⁰ for masking effects, and a model for computing the correlates of the color appearance attributes by Hunt.¹¹

By nature, a halftone pattern consists of signals of various spatial frequencies. As we shorten or enlarge the viewing distance, its power spectrum in the 2-dimensional spatial frequency domain would become narrower (shifting to lower frequencies) or broader (shifting to higher frequencies) accordingly. Because the human visual sensitivity depends strongly on the spatial frequency, the perceived halftone pattern and consequently the dot visibility are expected to vary with the changing viewing distance. Thus, the CSFs are crucial elements in the present study.

On the other hand, the masking affects account for the reduction of the signal at a given pixel by the signals (or more precisely the local contrasts) of its surround. The amount of reduction is proposed⁷⁻¹⁰ to be proportional to the linear summation of contrast energy weighted by spatial

pooling functions within a local region centered at the pixel of interest. For halftone patterns with low dot coverage, the effects of spatial pooling of the contrast energy from the surround is presumably small. Thus, the masking effects will be neglected in the present study and the simplified CVDP will be employed.

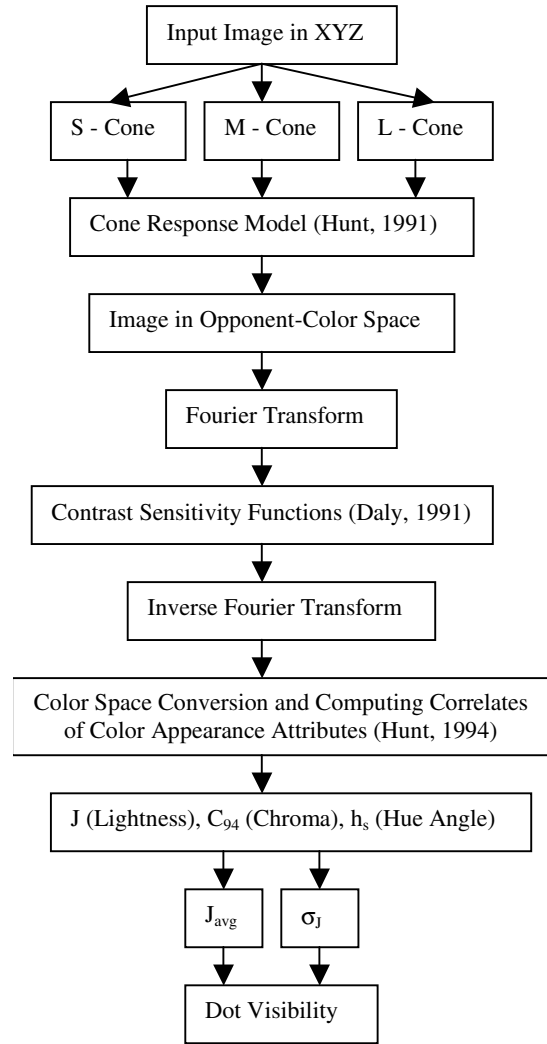


Figure 2. Flow chart of the simplified CVDP for dot visibility prediction.

As shown in Fig. 2, the simplified CVDP for the present study reads in an image in CIE 1931 tristimulus values XYZ . Details of the CVDP image processing algorithms can be found in Ref. 3. The model output is the perceived image in (J, C_{94}, h_s) or (lightness, chroma, hue angle) color space, from which the dot visibility metric can be computed.

Image Size and Resolution

To predict the threshold viewing distance for each halftone patch, we first need to determine the proper image

size and resolution to input to the model. The printer has a resolution of 600 dpi so that the side of each square micro-dot has a length $a = 42.3 \mu\text{m}$. The average dot diameter in Table 1 is $460.7 \mu\text{m}$. Thus, the printer uses roughly a 10 x 10 micro-dot to represent each dot on the first set of stimuli.

The print size of each halftone patch used in the experiment is about 5.5" x 5.5". It was found that even a 1" x 1" print would be adequate for the experiment. To avoid facing with excessive computing time, we choose an image size of 640 x 640 pixels.

Dot Representation

Each macro-dot (with diameter D of $460.7 \mu\text{m}$) on the first set of stimuli is described by the following azimuthally symmetric profile.

$$f(p) = 1 / \{ 1 + \exp [4(p - 3)] \}, \quad (3)$$

where p is the distance from the center of the dot in pixels. The normalized pixel value $N(x, y; D)$ at each pixel (x, y) is taken as the volume under the dot profile over the square of $x \pm 0.5$ pixel by $y \pm 0.5$ pixel.

For the second set of stimuli, $N(x, y; D)$ is equated to the fractional area of dot coverage at the pixel (x, y) . As shown in Fig. 3, the area coverage at each pixel can readily be computed once the areas of the shaded regions are known. The parameters α and β are the ratios of these areas to a^2 . ρ is the ratio of the dot diameter (D) to the ideal dot diameter ($a\sqrt{2}$). For non-overlapping dots ($\rho < 1$), we have

$$\alpha = \begin{cases} \frac{\rho^2}{2} \cos^{-1} \left(\frac{1}{\sqrt{2}\rho} \right) - \frac{1}{4} \sqrt{2\rho^2 - 1} & \text{when } \frac{1}{\sqrt{2}} \leq \rho < 1 \\ 0 & \text{when } \rho < \frac{1}{\sqrt{2}} \end{cases}, \quad (4)$$

and

$$\beta = \alpha - (\pi\rho^2) / 8 + 1/4. \quad (5)$$

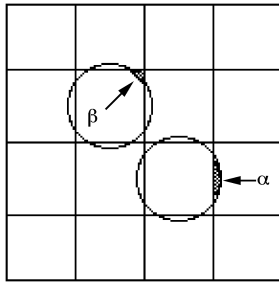


Figure 3. Definition of the area fractions α and β for the shaded regions.

The output from the printer is a laminated intermediate medium that is attached to a highly reflective white cardboard to create the test target for visual judgment. The spectral reflectance of a nonscattering uniform cyan patch with multiple reflections between the intermediate medium and cardboard can be expressed approximately as

$$R_c = R_f + [R_w + \frac{R_g \cdot (1 - R_w)^2}{1 - R_g \cdot R_w}] \cdot 10^{-2 \cdot D_{tc} \cdot C_c}. \quad (6)$$

Here R_f is the first surface reflectance, R_g the white cardboard reflectance, $R_w(\lambda)$ the spectral reflectance of the substrate of the intermediate medium, $D_{tc}(\lambda)$ the spectral transmission density of cyan dye, C_c the concentration of cyan dye, and λ the wavelength.

The spectra of R_w and D_{tc} are given in Fig. 4. Taking $R_f = 0.025$ and $R_g = 0.92$, we can compute the CIE tristimulus values ($\bar{X}YZ$) and visual density (D_v) at each level of dye concentration for the D50 illuminant. The results are summarized in Fig. 5 where the computed values of visual density match well with the measurements.

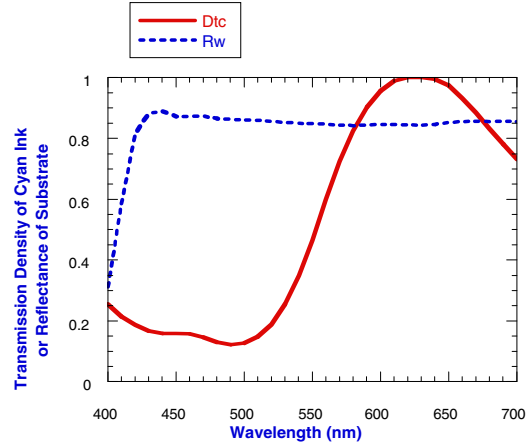


Figure 4. Spectral transmission density of the cyan ink and spectral reflectance of the substrate.

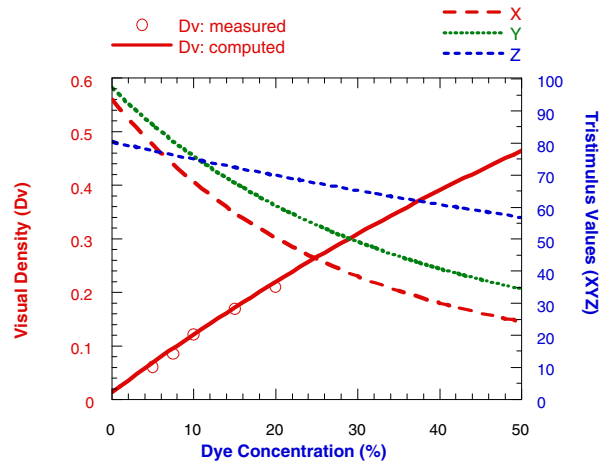


Figure 5. Variations of the measured and computed visual density values and computed tristimulus values with cyan dye concentration.

Predictions by the Simplified CVDP

If $N(x, y; D)$ represents a halftone image in normalized pixel value, then $C_c \cdot N(x, y; D)$ is the one in dye

concentration for each concentration level C_c specified in Table 1 or 2. The corresponding image in tristimulus values can be evaluated by using Fig. 5.

Once the halftone image is expressible in tristimulus values XYZ, it is ready to be processed by the simplified CVDP to obtain the corresponding images in perceived lightness and consequently the value of the metric C_j . Because the CSFs vary with the viewing distance (d) and XYZ depend on dot diameter (D) and visual density (D_v), we have $C_j = C_j(D, D_v, d)$.

Sub-images of 100x100 pixels in normalized pixel value and tristimulus Y value at a cyan dye concentration of 20% are shown in Fig. 6. The dot diameter is 461 μm . The corresponding sub-images in perceived lightness at viewing distances of 6", 10", 20", and 40" are given in Fig. 7. The variation of the perceived lightness and hence the dot visibility diminish as expected when the viewing distance is increased.

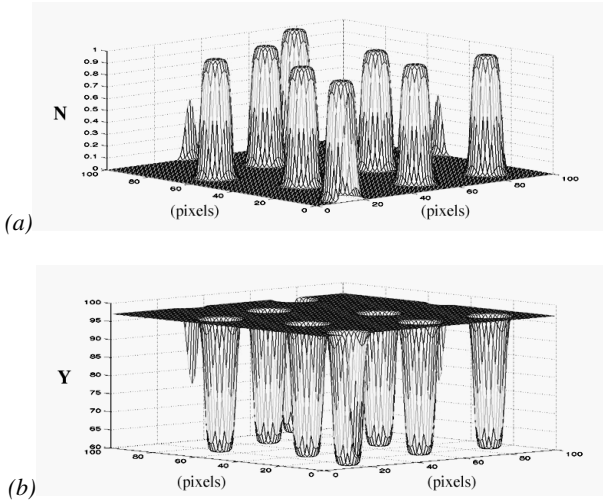


Figure 6. Samples of images in (a) normalized pixel value with dot diameter of 461 μm and (b) tristimulus Y value at dye concentration of 20%.

To determine the threshold metric value C_{JT} , we first establish the tables for C_j as a function of d for each test sample j using the simplified CVDP. These tables are expressible as

$$C_{ji}^{(j)} = C_j(D^{(j)}, D_v^{(j)}, d_i), \quad (7)$$

where $i = 1, 2, \dots, n$ with n being the number of entries in each table. In this study, we have found that the best fit between model predictions and experimental results can be achieved by choosing the threshold metric value as

$$\begin{aligned} C_{JT} &= C_j(D^{\#3}, D_v^{\#3}, d_T^{\#3} - \sigma_d^{\#3}) \\ &= C_j(460 \mu\text{m}, 0.121, 92.7'' - 7.3'') = 0.0021. \end{aligned} \quad (8)$$

Once C_{JT} has been determined, the threshold viewing for other patches can be computed by applying linear interpolation to tables specified by Eq. (7). The results for the first set of stimuli are given in Fig. 8 and those for the second set are summarized in Table 6. A threshold viewing distance of zero is assumed for a visual density of 0.05 that corresponds to the density of the white cardboard. The error bars in Fig. 8 show the ranges with one standard deviation from the mean.

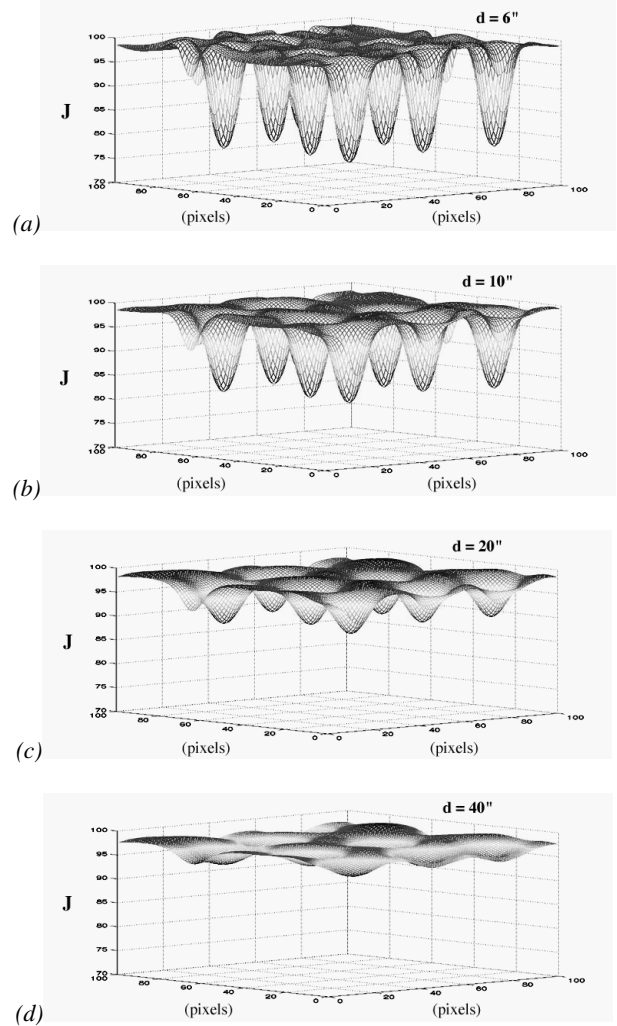


Figure 7. Samples of images in the perceived lightness with cyan dye concentration of 20% viewed at distances of 6", 10", 20", and 40", respectively.

Comparison with Measurements

In general, the predicted threshold distances agree well with the experimental results to within one standard deviation except for patch #1 from the printer and the sample with 10 pl drops from the breadboard. Nevertheless, predictions for both samples fall within two standard

deviation range from their respective measured results. In particular, the predicted threshold distance of 5.6" for the sample with 10 pl drops from the breadboard is very close to the measured distance of 4" to 5".

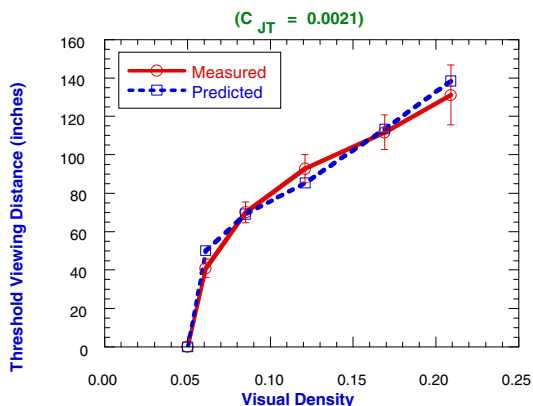


Figure 8. Comparison between predicted and measured threshold distances for samples from the printer. The error bars denote variations over one standard deviation.

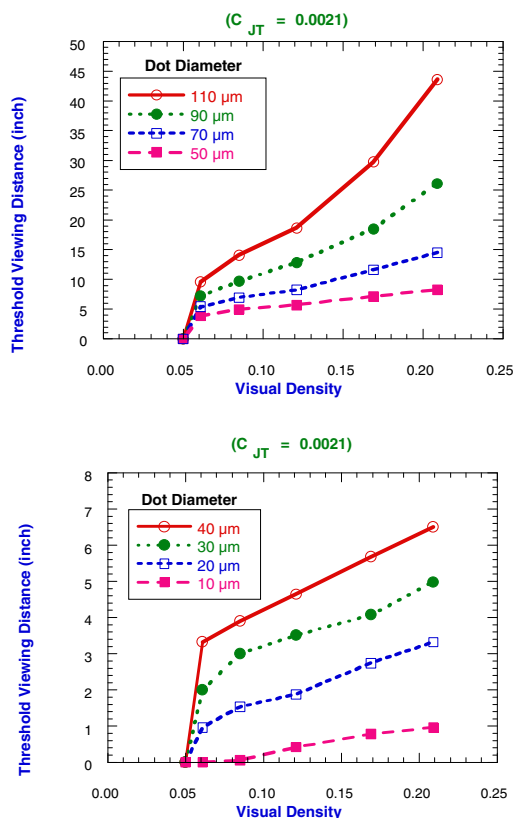


Figure 9. Model predicted threshold viewing distance as a function of dot diameter and visual density.

Table 6. Measured and Predicted Threshold Viewing Distances for the Second Set of Stimuli.

Patch	10 pl sample	20 pl sample	20 pl sample
Dot Diameter	53.9 μm	68.0 μm	76.0 μm
Measured	4" to 5"	9" to 10"	9" to 10"
Predicted	5.6"	7.9"	9.3"

On the other hand, the predicted distance of 7.9" for the sample with 20 pl drops from the breadboard is not as close to the measured distance of 9" to 10". This may be attributed to the uncertainty in determining the dot diameter. A previous experimental exploration on the morphology of ink dots generated by the breadboard indicated that the dot diameter should vary linearly with the square root of the drop volume. Thus the dot diameter for the 20 pl drop should be 76 μm instead of 68 μm. For this new dot size, the predicted threshold distance becomes 9.3", which falls right within the measured distance range of 9" to 10". These results are also included in Table 6.

The model predicted variations of threshold viewing distance with visual density at various dot sizes are given in Fig. 9 for halftone patches with 7% coverage of cyan dots. They provide useful information for selecting the proper concentration for the light cyan ink.

Concluding Remarks

In the present study, a metric (Eq. (2)) based on the human visual TVI curve and a visual processing model (the simplified CVDP in Fig. 2) is proposed to measure the ink dot visibility in a halftoned flat-field patch with low dot coverage. With the threshold metric value determined based on a single data point, the model predicted threshold viewing distances for halftone patches with various ink concentration and dot sizes are found to match reasonably well with the psychophysical test results (Fig. 8 and Table 6). The model predictions for the threshold viewing distance as a function of dot visual density and size (Fig. 9) should provide valuable guidance for choosing the proper settings for the drop size and ink density.

Acknowledgments

The authors are grateful to J. Seifl for providing the dot size and density measurements and to R. Miller and R. Reem for helpful discussions. They would also like to thank the seven subjects that participated in the psychophysical experiment.

References

1. Q. Yu, K. J. Parker, R. Buckley, and V. Klassen, A New Metric for Color Halftone Visibility, *Proc. PICS*, pg. 226 (1998).
2. M. Wang and K. Parker, A metric to evaluate the texture visibility of halftone patterns, *Proc. SPIE*, **4299**, pg. 163 (2001).

3. M. Lian, Image evaluation using a color visual difference predictor (CVDP), *Proc. SPIE*, **4299**, pg. 175 (2001).
4. R. W. G. Hunt, *Color Res. Appl.*, **16**, 146 (1991).
5. S. Daly, The Visible Difference Predictor: an Algorithm for the Assessment of Image Fidelity, in *Digital Images and Human Vision*, A. B. Watson, ed., MIT Press, Cambridge, MA, 1993, pg. 179.
6. A. B. Watson, *Comp. Vis. Graph. Image Proc.*, **39**, 311 (1987).
7. M. D'Zmura, Color Contrast Gain Control, in *Color Vision*, W. G. K. Backhaus, R. Kliegl, and J. S. Werner, eds., Walter de Gruyter, Berlin, 1998, pg. 251.
8. B. Singer and M. D'Zmura, *Vis. Res.*, **34**, 3111 (1994).
9. B. Singer and M. D'Zmura, *J. Opt. Soc. Am.*, **A 12**, 667 (1995).
10. M. D'Zmura and B. Singer, *J. Opt. Soc. Am.*, **A 13**, 2135 (1996).
11. R. W. G. Hunt, *Color Res. Appl.*, **19**, 23 (1994).

Biography

Ming-Shih Lian received the BS degree in Nuclear Engineering from National Tsing-Hua University in Taiwan in 1970 and the PhD degree in Mechanical Engineering from State University of New York at Stony Brook in 1978. Prior to joining Eastman Kodak Company in 1983, he worked on system modeling and simulation in Combustion Engineering, Inc. and Xerox Corporation. His recent work involves image chain simulation, color visual processing, and digital color halftoning.